Advanced Course and Workshop on Blood Flow
BF 2005 – (pp.273–298) – Warsaw, 2005.

Concepts for High Resolution Blood Flow Imaging with High Frequency Ultrasound

Michael Vogt

Institute of High Frequency Engineering
Ruhr-University Bochum, IC 6/133,
44780 Bochum, Germany
Michael.Vogt@rub.de

In this paper the design of a high frequency ultrasound (HFUS) pulsed wave Doppler (PWD) system for blood flow imaging in small vessels is presented. High frequency and broadband ultrasound in the 50 MHz range is utilized in order to obtain a good spatial resolution. Echo signals are analyzed making use of combined time/frequency domain approaches for axial blood flow velocity estimation. Furthermore, an approach for the estimation of the radial blood flow velocity component with rotational symmetric sound beams is presented. With the help of these approaches, the magnitude and sign of the axial flow velocity in sound propagation direction and the magnitude of the velocity component perpendicularly are accessible. The implemented PWD system and the proposed flow estimation approaches have been tested with the help of simulations and flow phantom measurements. Results of the system's validation and results of in vivo images on small blood vessels are presented.

Key words: *High frequency ultrasound, blood flow, pulsed wave Doppler*

1. Introduction

Ultrasound Doppler systems enable the assessment of blood flow in organs and vessels by measuring blood flow velocities and perfusion [1]. In dermatology and other applications, small vessels with low blood flow velocities are of special interest [2–6]. High resolution and robust flow estimation concepts have to be applied under these conditions.

A PWD system with a high frequency spherically focused single element transducer (50 MHz center frequency, 80% relative bandwidth) has been designed and implemented. A waveform generator is utilized for transmit signal

generation, and radio frequency (RF) echo signals are directly digitized with a transient recorder. Periodic sequences of pulsed signals are transmitted with an adjustable and predefined pulse repetition frequency (PRF) at discrete lateral transducer positions for flow and perfusion imaging across blood vessel's cross sections [6–13]. Flow in vessels can be separated in axial and radial flow velocities components in sound propagation direction and transversely, respectively, in the context of the utilized spherically focused single element transducer [8, 10–11].

Consecutive sequences of echo signals are acquired over time of flight ("micro time axis") and over repeated pulse transmissions ("macro time axis"). Digitized data is represented in the two dimensional micro/macro time axis space, which enables an easy interpretation and motivation of different concepts for blood flow velocities estimation. Conventional frequency domain and time domain approaches as well as time/frequency domain approaches for the estimation of axial blood flow velocities are discussed. Trade-offs between a good spatial resolution and a good velocity resolution are analyzed. It is shown that combined time/frequency domain approaches can advantageously be applied in the context of broadband systems [7, 9, 12]. Furthermore, an approach for the estimation of the magnitude of radial flow velocities is proposed. The statistics of echo signals from blood, which transversely cross the sound beam, is analyzed in this approach [8, 10–11, 14–15].

Implementations of wall-filters, which are utilized to suppress the stationary echoes from the non moving tissue, that are significantly larger than the echoes from blood, are discussed. Power-mode images and color flow images are calculated off-line.

Simulations and flow phantom measurements have been performed in order to test and validate the implemented PWD system and the proposed flow estimation strategies. Furthermore, in vivo measurements on small blood vessels at the back of a human hand have been performed. It will be shown that the implemented system is capable of detecting and measuring blood flows in small vessels with diameters down to 100 μm with flow velocities in the range of some few mm/s.

2. High Frequency Ultrasound for High Resolution Blood Flow Imaging

A sufficiently good spatial resolution has to be achieved and sensitive flow estimation approaches have to be applied for blood flow imaging in small vessels with very small diameters and very small blood flow velocities. High frequency and broadband ultrasound in the 50 MHz range is utilized to fulfill these requirements.

2.1. Measurement Configuration

Because HFUS arrays operating at frequencies above 30 MHz are not yet available, a spherically focused single element transducer is utilized for the measurements. The measurement configuration is shown in Fig. 1.

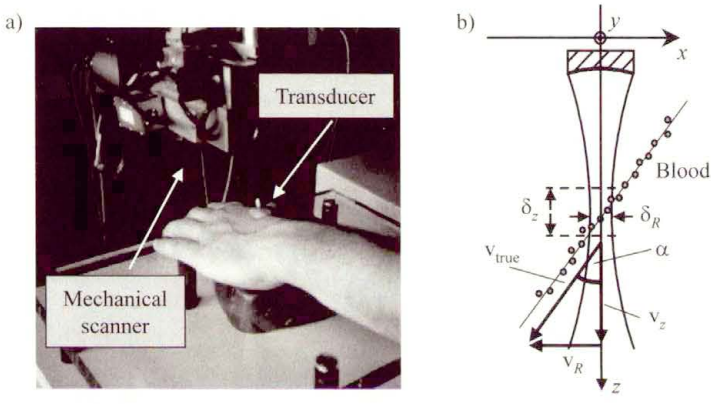

FIGURE 1. a) measurement setup, b) flow geometry: true flow velocity v_{true}, axial and radial flow velocities v_z and v_R.

Movement artifacts, which might occur during in vivo measurements, have to be avoided. A mechanically stable measurement platform that fixes the transducer relative to the blood vessels under investigation, see Fig. 1 a), has been designed. The transducer is positioned above the blood vessel, whereby an angle α between the direction of sound propagation (axial direction) z and the flow direction is given, see Fig. 1 b). Ultrasound gel is used as sound propagation medium between the transducer and the tissue. For morphological skin imaging with HFUS, usually water is used as coupling medium. This is achieved by mechanically scanning the transducer inside a water bath inside a small tank with a slot at the bottom side, which is

placed on the skin surface [6, 16–18]. But this is not appropriate for blood flow measurements because blood flow inside the small vessels would collapse under the mechanical load. For this reason, ultrasound gel is used as sound propagation medium. Air bubbles, which might be present in the gel, significantly disturb the propagation of HFUS. Hence, air bubbles have to be avoided as much as possible.

The ultrasound waves, which are emitted by the transducer, are backscattered at the moving blood particles, mainly the erythrocytes, inside the blood plasma. Because a rotational symmetric ultrasound transducer with a narrow sound beam is utilized for imaging, the true velocity v_{true} of moving blood particles can be separated into the axial flow velocity v_z in axial direction z and in a flow velocity v_R in the radial direction R perpendicularly to the direction of sound propagation, see Fig. 1 b).

$$v_z = v_{\text{true}} \cos\alpha\,, \quad v_R = v_{\text{true}} \sin\alpha\,, \quad v_{\text{true}} = \sqrt{v_z^2 + v_R^2}\,. \tag{2.1}$$

The magnitude and the sign of the axial flow velocity v_z can be estimated, i.e. blood flow towards the transducer and that away from it can be distinguished from each other and quantified with the signal processing concepts introduced below. It will be shown that the radial traverse of blood particles through the sound beam causes a modulation of the echo signal. This modulation can be analyzed in order to estimate the radial flow velocity v_R. Given the rotational symmetry of the transducer, it is evident, even at this point, that the *direction* of the radial flow cannot be measured.

The transducer is mechanically scanned along the lateral direction x and measurements are repeated with the transducer being stopped at discrete lateral positions x_n to obtain spatially resolved flow measurements.

2.2. Pulse Echo Measurements Utilizing High Frequency Ultrasound

A spherically focused ultrasound transducer is utilized for all measurements in order to achieve a high measurement sensitivity and a good radial resolution. Pulse echo measurements are performed emitting pulsed ultrasound waves, which propagate along the pencil-like sound beam. Ultrasound waves, which are backscattered at acoustical inhomogeneities inside the tissue and at the moving blood particles, are received by the same transducer. The resulting radio frequency (RF) echo signal is directly sampled over time

of flight (TOF). Under these conditions, the spatial resolution δ_R of the system in radial direction R depends on the sound field characteristics, i.e. on the focusing, the transducer's center frequency f_0 and the aperture diameter D. The system's capability to separate scatterers along the sound beam analyzing echo signals over TOF, i.e. the axial resolution δ_z in the direction of sound propagation z, depends on the transducer's bandwidth B [6, 16–17]:

$$\begin{aligned} \delta_R &= \frac{c}{f_0} F \approx 1600\,\mu\mathrm{m} \frac{1}{(f_0/\mathrm{MHz})} F, \\ \delta_z &= \frac{2c \ln 2}{\pi B} \approx 706\,\mu\mathrm{m} \frac{1}{(B/\mathrm{MHz})}\,. \end{aligned} \tag{2.2}$$

In Eq. (2.2) $c \approx 1540\,\mathrm{m/s}$ is the speed of sound and $F = z_0/D$ denotes the 'f-number' with the focus length z_0 and the aperture diameter D. The dispersive nature of the tissue attenuation happens to be remarkably prominent in the case of high frequency broadband ultrasound, making it strongly frequency dependent. Because the attenuation increases with increasing frequency, echo signals are shifted down regarding center frequency and bandwidth with increasing depth. Consequently, radial and axial resolutions are degraded over depth [6, 16–17].

2.3. Echo Signal Acquisition for Blood Flow Measurements

Pulsed signals are emitted for spatially resolved measurements along the axial direction. Echo signals, which are backscattered at moving blood particles inside the transducer's sound beam, show a Doppler shift relative to the transmit signal.

A single moving scatterer with a constant axial flow velocity v_z is considered for an analytical description, first. With the speed of sound c and the system's impulse response $h(t)$, the scatterer's axial position $z(t)$ over time and the relationship between the transmit signal $s_T(t)$ and the echo signal $s_E(t)$ are:

$$\begin{aligned} z(t) &= z_0 + v_z t\,, \qquad & s_E(t) &= h(t) * s_T(a(t - t_0))\,, \\ a &= 1 - \frac{2v_z}{c}\,, & t_0 &= \frac{2z_0}{c}\,. \end{aligned} \tag{2.3}$$

Because blood flow velocities are much smaller than the speed of sound, the scaling factor in Eq. (2.3) is very close to one, i.e. $a \approx 1$. Consequently,

long-term observations have to be performed to be able to estimate the axial flow velocity v_z.

In order to analyze the Doppler shift due to the axial scatterer movement the concept of *continuous wave Doppler (CWD) systems* is considered first [1]. In this approach, a sinusoidal continuous wave (CW) transmit signal $s_T(t)$, i.e. a narrowband signal at angular frequency ω_0, is emitted from a transducer. The echo signal $s_E(t)$, which is caused by backscattering at moving blood particles, is received with another transducer, that is located closely beside the first one, and shows an angular Doppler frequency shift ω_D. The analytical transmit signal $s_{T+}(t)$ and analytical echo signal $s_{E+}(t)$ are given by the following relationships, see Eq. (2.3):

$$s_{T+}(t) = A_0 e^{j\omega_0 t}, \quad s_{E+}(t) = A_0' e^{j(\omega_0 - \omega_D)t}, \quad \omega_D = \omega_0 \frac{2v_z}{c}. \tag{2.4}$$

The Doppler frequency ω_D is proportional to the axial flow velocity v_z, and is very small compared to the angular frequency ω_0, which is chosen to be the transducer's center frequency. Usually, the echo signal is quadrature demodulated, i.e. mixed with the CW transmit signal downwards to the base band. As a result, the quadrature demodulated signal (I/Q-signal: in-phase/quadrature phase signal) $s_D(t)$ is obtained:

$$s_D(t) = s_{E+}(t) e^{-j\omega_0 \cdot t} = A_0'' e^{-j\omega_D \cdot t}. \tag{2.5}$$

Assuming $s_D(t)$ to be analyzed over a long time interval, a spectral analysis delivers directly information about the distribution of axial flow velocities inside the intersection of the two transducer's sound beams [1].

In *PWD systems*, on the other hand, broadband pulsed signals with a *short pulse duration* are emitted in order to obtain a good axial resolution, as motivated above. If only a *single* pulsed signal is emitted, the scaling of the echo signal in Eq. (2.3) is too small to be analyzed with respect to the axial flow velocity v_z. For this reason, *trains of consecutive broadband pulses* with an adjustable and predefined PRF $f_{PRF} = 1/T$ are emitted in PWD systems [1, 2–3, 7].

While the TOF of the ultrasound waves from the transducer to the backscattering structures and back is on the order of several μs, the PRF is some orders of magnitude higher, i.e. on the order of several ms. The analysis of the consecutive echo signals, which are caused by the consecutively

emitted transmit pulses, enables a long-term observation of moving scatterers. It is already evident from this description that a sampling procedure is involved in this approach. In Fig. 2, a simulated sequence of RF echo signals for one single point-like moving point scatterer inside the transducer's sound beam is shown.

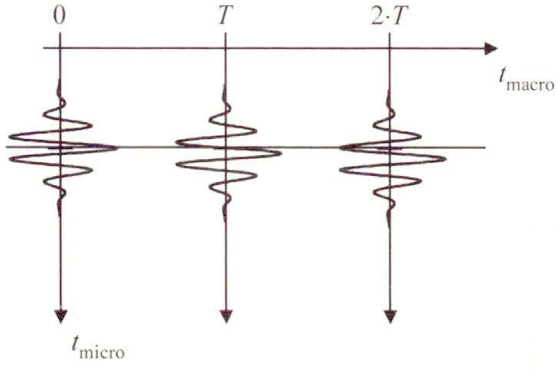

FIGURE 2. Simulated sequence of RF echo signals for one single point-like moving scatterer

In the simulation, a fractional bandwidth $B/f_0 = 80\,\%$, i.e. a very broadband system, was presumed. The above described PWD concept is analogous to a stroboscopic measurement setup with a periodically triggered flashlight, which illuminates a moving object. With each flash, a "snapshot" is obtained, i.e. the object's movement is sampled over time. Consequently, the PRF is a crucial parameter, which determines the maximum unambiguously measurable axial flow velocity $v_{z,\max}$ in PWD systems [1]:

$$v_{z,\max} = \frac{c}{4}\,\frac{f_{RPF}}{f_0}\,. \tag{2.6}$$

In Fig. 2 the consecutive echo signals, which result from each pulsed transmit signal, are shown side by side. In this representation, the "micro time axis" is equivalent to the TOF, which is, scaled by the speed of sound c, proportional to the axial coordinate z. Consecutive transmissions with the given PRF define the "macro time axis" with a sampling from pulse to pulse. It can be seen that the axial scatterer movement results in an echo signal movement along the micro time axis for consecutive pulses along the macro time axis. Below, this circumstance is utilized to estimate the scatterer's axial flow velocity. Whereas only a single point-like scatterer was considered so far, the echo signal from blood is caused by the superposition of the ultrasound waves

that are backscattered at many individual blood particles. Consequently, the "speckle" texture, which is very typical for ultrasound images, is also found in the echo signal sequences that are caused from backscattering at blood.

3. High Frequency Ultrasound Pulsed Wave Doppler System Implementation

The block diagram of the implemented PWD system is shown in Fig. 3.

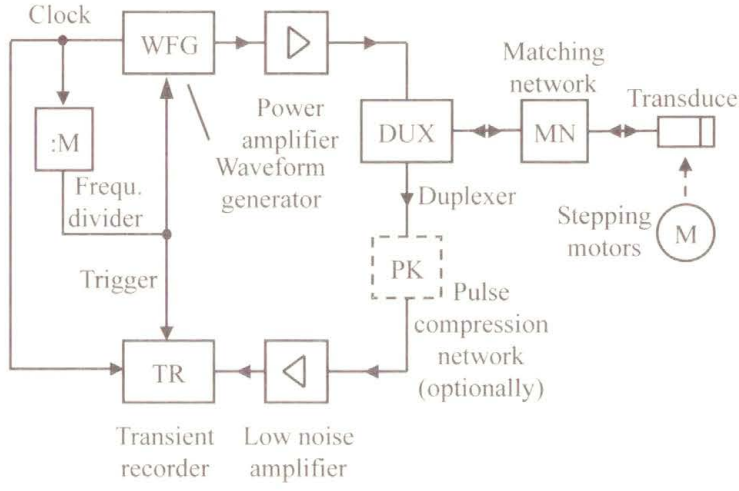

FIGURE 3. Block diagram of the implemented PWD system

The single element transducer is excited with a transmit signal, which is generated by a waveform generator (WFG; Model 2045 polynomial waveform synthesizer, Analogic Inc., USA: 500 MHz maximum sampling frequency, 8 bit amplitude resolution) with a subsequent power amplifier (Model 250L, Amplifier Research Inc., Souderton, PA, USA). Arbitrary signals within a limited bandwidth can easily be generated feeding digitized data of a desired signal into the WFG. In the receive path, the RF echo signal is amplified with a low noise amplifier (AU-1301, Miteq Inc., Hauppauge, NY, USA: 30 dB gain). Thereafter, the RF signal is directly sampled and digitized with a transient recorder (TR; RTD 720, Tektronix Inc., Beaverton, OR, USA: 500 MHz sampling frequency, 8 bit amplitude resolution). Pulse echo measurements are performed, i.e. the same transducer is utilized for transmission and reception of ultrasound waves. A duplexer (DUX) is utilized to actively switch

the transducer between the transmitter during signal transmission and the receiver during echo signal reception.

It is essential to synchronize the transmitter and the receiver in the PWD system in order to acquire the echo signal sequences in an appropriate way. Furthermore, a well defined and adjustable PRF is required. For these reasons, the clock signal of the WFG is connected with the external clock input of the TR. Furthermore, both devices, the WFG and the TR, are triggered with the same signal, which is derived from the clock signal with an adjustable frequency divider. The PRF is thus an integral divider of the 500 MHz clock signal, see Fig. 3. With each trigger event, a pulsed transmit signal is emitted and the resulting RF echo signal is acquired after a constant time delay, which is adjustable in the WFG.

The electrical matching between the transducer and the driving electronics can be improved with an optional matching network between the DUX and the transducer. A reactance matching network was specially designed for this purpose. However, the design of a *broadband* matching network is a difficult and challenging task. Consequently, the system's bandwidth is lower with the network than without it [16]. The transducer can be mechanically scanned in the two orthogonal directions in the horizontal plane using two stepping motors (Iselautomation KG, Eichenzell, Germany). A controlled DC-motor (Physik Instrumente GmbH, Karlsruhe, Germany) is utilized to mechanically move the transducer in axial direction. This allows the positioning of the transducer's focus in a desired depth, which is usually the center of the region of interest (ROI). In Fig. 4, a photograph of the implemented PWD system is shown.

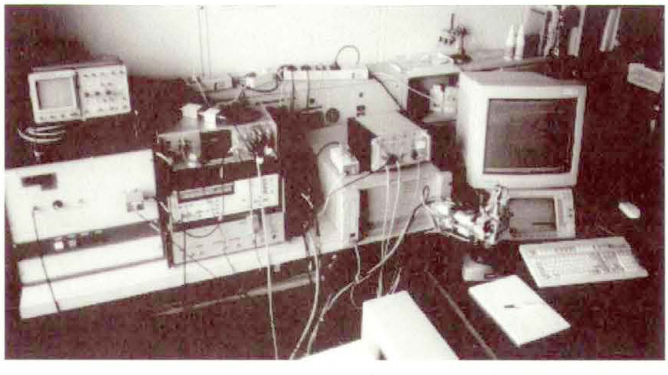

FIGURE 4. Photograph of the implemented PWD system

4. High Resolution Blood Flow and Perfusion Imaging

The acquired echo signal sequences are analyzed with the aim to quantify blood flow velocities and perfusion with a high resolution. Appropriate estimation approaches are required in the context of very broadband signals, which are applied in the implemented PWD system. Spatial and velocity resolution, i.e. the system's ability to spatially resolve flow conditions and to differentiate flow velocities, are crucial parameters in this context.

4.1. Parameters for the Quantification of Blood Flow and Perfusion

In contrast to the *morphological* nature of B-mode (B: "brightness") imaging of biological tissues Doppler techniques allow for *functional imaging*, i.e. they enable to quantify blood flow. Though several parameters like flow velocities profiles, mean flow velocities, volume flow, quantified turbulences, etc. are of interest from the physiological point of view, not all of them are directly accessible with ultrasound. Furthermore, a suitable visualization of measured data is an important issue in the medical application. The following flow visualization modalities are typically applied in medical sonography [1]:

- **Duplex mode:** The axial flow velocity *distribution* of blood particles inside one single point of interest is estimated and visualized over time. This allows to analyze flow velocity changes over time in great detail.
- **Color flow mapping (CFM):** *Mean* axial flow velocities of blood particles are estimated point-wise in a user-defined ROI. Estimated mean axial velocities are visualized in a color-coding scheme and superimposed to a grayscale B-mode image. This facilitates a detailed analysis of the *spatial* distribution of mean flow velocities over time.
- **Power mode:** The *energy* of signals, which are backscattered at moving blood particles, is point-wise estimated in a user-defined ROI, and results are visualized in a color-coding scheme. The perfusion of organs can be analyzed in this mode. Blood flow is only qualitatively visualized and no information about flow velocities is included.

The schematic in Fig. 5 shows the relationship between the different parameters and the actually given distribution of axial flow velocities. It is assumed, that the likelihood $L(v_z)$ for a given axial flow velocity v_z is estimated at each point of interest along the z axis. In the figure, $L(v_z)$ is normalized to its maximum.

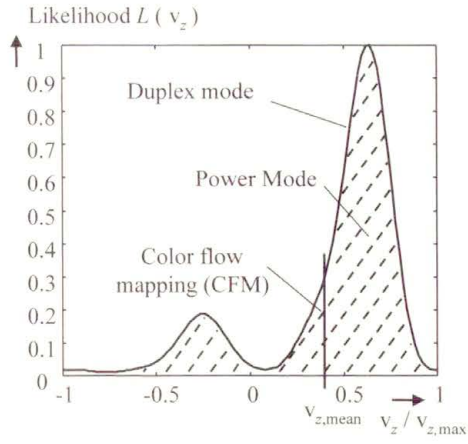

FIGURE 5. Parameters and imaging modalities for flow and perfusion quantification

For color flow mapping the mean flow velocity, $v_{z,\mathrm{mean}}$ is calculated as the centroid, i.e. the first moment over the zero order moment, of the velocity distribution $L(v_z)$:

$$v_{z,\mathrm{mean}} = \frac{\int v_z L(v_z)\,\mathrm{d}v_z}{\int L(v_z)\,\mathrm{d}v_z}\,. \tag{4.1}$$

Several approaches for the estimation of the axial flow velocity distribution as well as an approach for the estimation of the mean radial flow velocity component with rotational symmetric sound beam transducers are discussed below.

4.2. Axial Flow Velocity Estimation

It was already discussed above that the flow of scatterers along the axial coordinates results in a movement of consecutive echo signals along the micro time axis from pulse to pulse, see Fig. 2. Conventionally, sequences of *narrowband* burst signals, i.e. trains of low-frequency pulsed signals, that modulate the amplitude of a carrier signal at the system's center frequency f_0, are transmitted in PWD systems. Under these conditions, the axial flow velocity distribution can be estimated sampling the sequence of quadrature demodulated echo signals at *constant* lags on the micro time axis for consecutive pulses along the macro time axis. Employing the fast Fourier transform (FFT) of sampled data, estimates for the axial flow velocity distribution in

each depth along the sound beam are obtained (FFT-approach) [1, 7]. Because spectral information is analyzed, this procedure can be classified as a *frequency domain* approach. Kasai et al. proposed a very efficient technique for estimating the mean axial flow velocity analyzing the autocorrelation function of sampled data [19].

However, these approaches are not appropriate in the context of *broadband* transmit signals, which are utilized in the implemented PWD system in order to obtain a good spatial resolution in the axial direction of sound propagation. The reason for this is that the envelope of the short duration pulsed signals significantly passes through the range gates from pulse to pulse, i.e. through the points at constant depths along the micro time axis. This can be seen in Fig. 6, which shows another simulated echo signals sequence for six discrete moving point-like scatterers with different axial flow velocities. For the simulation, again, a very broadband system with a fractional bandwidth $B/f_0 = 80\,\%$ was presumed:

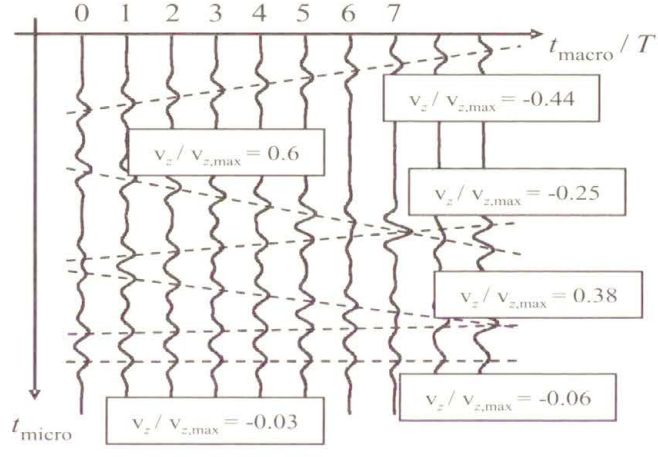

FIGURE 6. Simulated sequence of RF echo signals for 6 discrete single point-like moving scatterer [7]

The axial scatterer movement can be observed over a very small number of pulses only by sampling the echo signals sequence at constant lags on the micro time axis. As a result of this, a *spectral broadening* occurs applying the FFT approach, what is the more distinct the higher the axial flow velocity is. For this reason, the axial flow velocity resolution, which quantifies the system's ability to resolve different axial flow velocities, is the worse the higher the axial flow velocity is [7].

More recently, new approaches for the analysis of the RF echo signals in the *time domain* have been introduced. The *mean* axial flow velocity of moving blood particles is analyzed by calculating the cross correlation function of consecutive RF echo signals, i.e. of signals recorded along the micro time axis, for consecutive pulses along the macro time axis (RF-CC approach: Radio frequency cross correlation). Because the axial scatterer movement is directly estimated by analyzing the time domain characteristics of the echo signals, this technique is classified to be a *time domain* approach. This approach, however, suffers the drawback of estimating merely the means axial flow velocity instead of the more desirable velocity distribution.

The pulsed echo signals sequence for single point-like scatterer, which move with a constant axial flow velocity along the sound beam, shows a constant time shift from pulse to pulse along the micro time hence the scatterer moves along *lines of constant inclination* in the two-dimensional micro and macro time axes space, see Fig. 6. Consequently, the axial scatterer movement can be tracked by sampling the sequence of echo signals along trajectories, which correspond to different axial flow velocities. For each trajectory, the likelihood for given scatteres with a corresponding axial flow velocity is estimated. This is done by analyzing the sampled RF echo signal or the sampled quadrature demodulated signal (WMLE approach: wideband maximum likelihood estimator/Butterfly Search Algorithm [6–7, 20–23]). Because spectral and time domain information is combined in these approaches, they are classified as *combined time/frequency domain* approaches, here [12].

Figure 7 shows the estimated axial velocity distributions for the echo signals sequence that are shown in Fig. 6. Results obtained with the FFT approach and with the Butterfly Search Technique are shown [7].

It can be seen that the axial resolution and the axial velocity resolution, which quantifies the system's capability to distinguish the axial positions and axial flow velocities of moving scatterers, are better with the Butterfly Search Technique than with the FFT approach. Furthermore, utilizing the FF, spatial and velocity resolutions depend on the axial flow velocities [6–7]. This is due to enlarged spectral broadening brought about by shorter times of observation, in which the scatterer movement can be analyzed.

In conclusion, the tracking of the axial scatterer movement in the context of the Butterfly Search approach enables a long-time analysis of the echo signals sequence along the macro time axis independent of the transmit signal pulse width. Consequently, axial flow velocity distribution estimates have

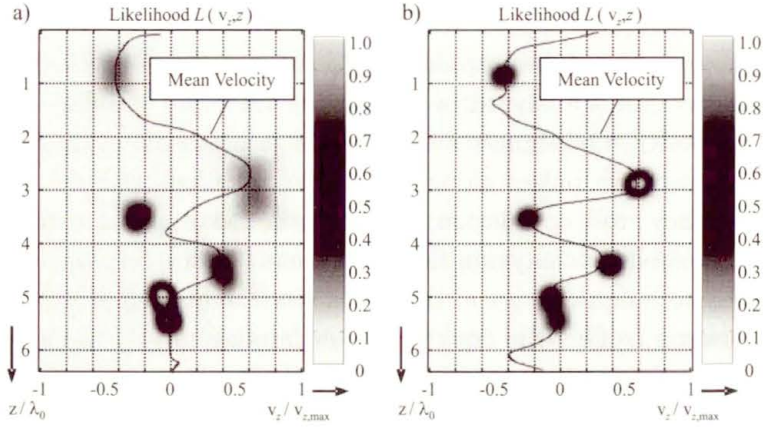

FIGURE 7. Estimated axial velocity distribution: a) FFT approach, b) Butterfly Search Technique [7]

a lower variance with the Butterfly Search approach than with the FFT approach albeit at the expense of much higher computational cost.

4.3. Radial Flow Velocity Estimation

So far only axial scatterer movements in the direction of sound propagation were considered and it was assumed that the scatterers movement in transverse direction is of no further consequence. Actually, the traverse of blood particles through the sound beam causes a modulation of consecutive echo signals from pulse to pulse.

With the given rotational symmetry of the sound beam of the spherically focused transducer's sound beam, it is assumed that the point spread function (PSF) $h(t, z', R')$, which is the system's response for a single point-like scatterer at an axial and lateral position $z = z'$ and $R = R'$, is separable into an axial component $h_z(t, z')$ and a radial component $h_R(R', z')$:

$$h(t, z', R') = h_z(t, z')\, h_R(R', z')\,. \tag{4.2}$$

The system's response regarding axial scatterer movements was already discussed above. If the scatterers pass the sound beam in transverse direction, see Fig. 1 b), and if the observation time is sufficiently large, a significant modulation of the echo signals sequence along the macro time axis is caused. This modulation depends on the transducers' sound field characteristics. The magnitude of the radial flow velocity v_R can be estimated with measurements

of the PSF as a reference. However, the *direction* of the radial flow cannot be measured with the rotational symmetry of the sound beam. Because of the speckle texture, which is inherent in the echo signals backscattered at moving blood particles, the speckle statistics has to be analyzed. In the proposed estimation approach, this is performed analyzing the auto-covariance function (ACVF) of the echo signals envelope [8, 10–11].

Again, simulated echo signals sequences have been utilized to establish and to evaluate the estimation approach. The simulations were based on the geometry in Fig. 8.

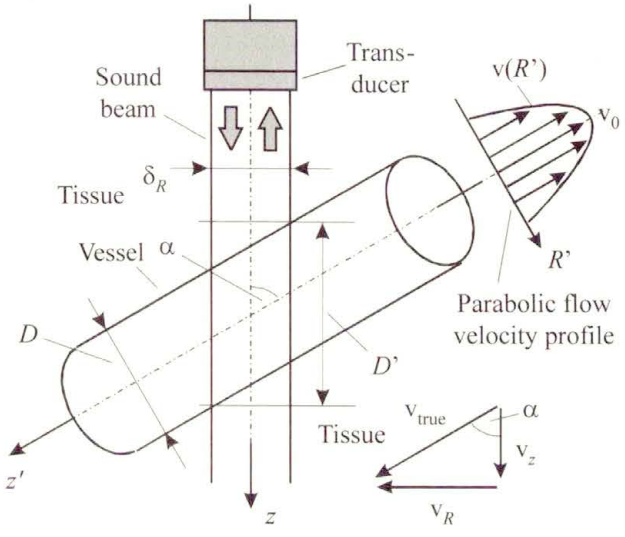

FIGURE 8. Flow simulations: Vessel diameter D, insonation angle α

Laminar flow with a parabolic true velocity profile inside a vessel with a given diameter D was assumed. Furthermore, uniformly distributed point-like scatteres were assumed to be located inside the vessel. As an example Fig. 9 shows a simulated echo signals envelope sequence for a single transducer position.

An incident angle $\alpha = 90°$, i.e. a transverse flow relative to the direction z of sound propagation, was chosen. The system's axial and radial resolution in the simulation were 17 μm and 54 μm respectively like in the implemented PWD system. A vessel diameter $D = 450\,\mu$m, a peak flow velocity of $v_{\text{true,max}} = 22$ mm/s and a PRF $f_{\text{PRF}} = 3200$ Hz was assumed. A number $M = 50$ of echo pulses was simulated, i.e. the observation time was about 16 ms.

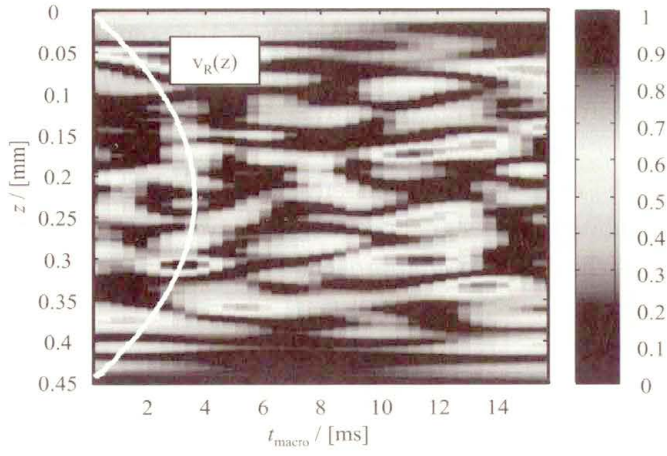

FIGURE 9. Simulated echo signals envelope sequence

It can be seen in Fig. 9 that the given speckle pattern decorrelates fastest in the center of the vessel, where the radial flow velocity is the largest. On the other hand, the echo signals are almost stationary at the vessel walls because the flow velocity reaches zero, i.e. no scatterer movement is given. Consequently, the rate of the decorrelation of echo signals along the macro time axis is a measure for the magnitude of the radial flow velocity. However, the actual sound beam characteristics, i.e. the radial component $h_R(R', z')$ of the PSF, see Eq. (4.2), has to be known.

Calibration measurements have been performed to measure the system's PSF. A tungsten wire with a $7\,\mu$m diameter, which is significantly smaller than the transducer's axial and radial resolution and the wavelength at the system's $f_0 = 50\,$MHz center frequency, was utilized as a point-like imaging object. Because of the focused sound beam characteristics, which significantly changes over depth z, see Fig. 1 b), the wire was imaged in several depths [8, 10-11, 16].

The mean radial flow velocity is estimated in each depth z analyzing the envelope of the echo signals sequence along the trajectory in the micro and macro time axis space that corresponds to the estimated mean axial flow velocity at the same depth. The decorrelation of speckle is analyzed by calculating the ACVF of the sampled data, see Fig. 10.

The ACVF of the B-mode data of the measured PSF is utilized as reference. The ACVF of measured data is a replica of the ACVF of the radial

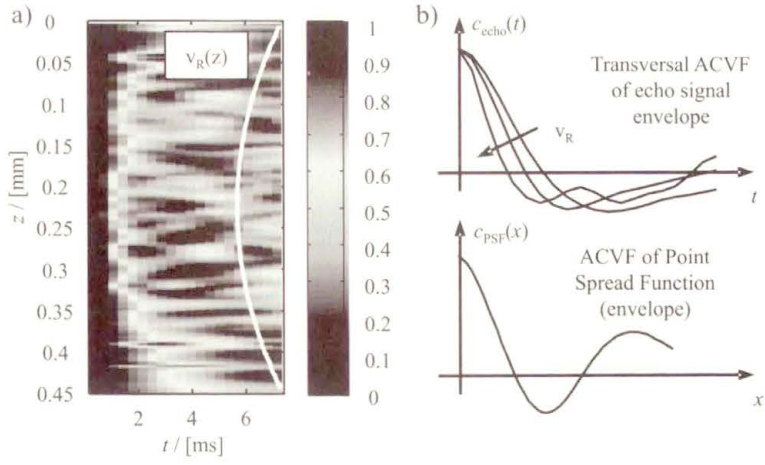

FIGURE 10. a) ACVF of echo signal envelope over depth z, b) connection between ACVF of echo signal envelope and ACVF of measured PSF

component $h_R(R', z')$ of the PSF, which is scaled by the unknown mean radial flow velocity v_R [8, 10-11]:

$$c_{PSF}(x) = c_{\text{echo}}(v_R t)\,. \tag{4.3}$$

The estimated mean radial flow velocities over depth are shown in Fig. 11. The radial flow velocity profile is reconstructed under the simulated conditions, but the variance of flow velocity estimates is relatively high.

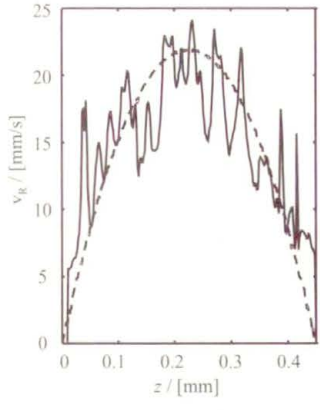

FIGURE 11. Estimated radial flow velocity over depth

4.4. Stationary Echo Cancellation and Perfusion Estimation

Echo signals, which result from backscattering in the tissue, are stationary signals, i.e. they do not change from pulse to pulse as long as movement artifacts can be neglected. In contrast, echoes from the backscattering at moving blood particles change from pulse to pulse along the macro time axis. Because echoes from blood are significantly smaller than the echoes from the tissue, it is desirable to suppress the stationary echoes prior the estimation of flow velocities. Furthermore, if echoes from backscatter at blood are separated from backscatter from the tissue, the signal energy is a parameter for perfusion imaging, which is utilized for power mode imaging.

Making use of the fact that stationary echoes are constant components of the sampled data along the macro time axis for constant lags on the micro time axis, i.e. at constant depths z, this suppression can be performed by digital filtering. The "*wall-filter*" has to be a digital high-pass filter. If a finite impulse response (FIR) filter of an *odd* order N is applied, the relationship between the digital input signal x_n and the digital output signal y_n can be described as follows:

$$y_n = \sum_{i=0}^{N} h_i \, x_{n-i}, \quad \text{with: } h_i = -h_{N-i} \, . \tag{4.4}$$

The impulse response in Eq. (4.3) ensures that a constant input signal x_n results in an output signal $y_n = 0$, what is desired in order to suppress the stationary echo signals. In Fig. 12 the magnitude of the filter's transfer function is shown for different filter orders N and for the approximation of a rectangular transfer characteristics with a cut-off-frequency corresponding to an axial cut-off flow velocity $v_{z,\mathrm{cut}} = 0.1 \cdot v_{z,\max}$.

Another possible wall-filter implementation, which is a very straight forward approach, is to estimate the mean value of the input signal sequence x_n, $n = 1, 2, \ldots, M$, which is utilized for velocities estimation. At the wall-filter's output, the following signal sequence y_n is assigned:

$$\bar{x} = \frac{1}{M} \sum_{i=1}^{M} x_i, \quad y_n = x_n - \bar{x}, \quad n = 1, 2, \ldots, M \, . \tag{4.5}$$

The relationship between the wall-filter input and output in Eq. (4.5) is a non-causal relationship.

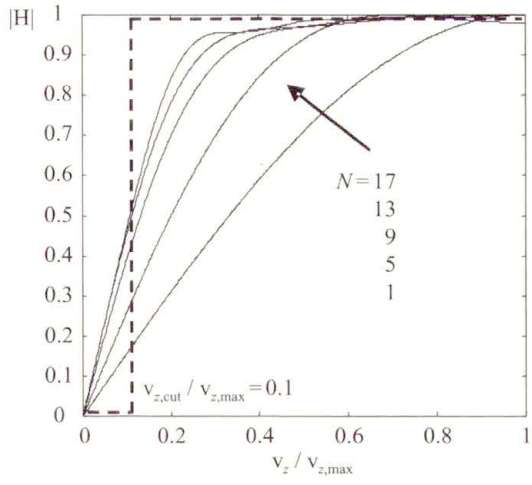

FIGURE 12. Wall-filter transfer function (magnitude) for different filter orders N

5. Flow Phantom Measurements

Flow phantom measurements have been performed in order to evaluate the proposed PWD system and the proposed approaches for flow velocities estimation. Equivalent to the simulations discussed in the context with Fig. 8, it was intended to perform the measurements under well defined conditions. Flow phantoms were specially designed for this purpose, see Fig. 13.

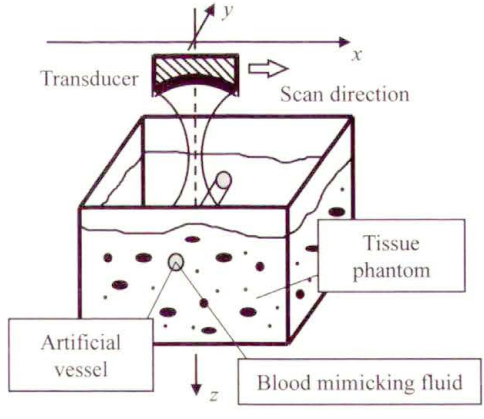

FIGURE 13. Flow phantom: artificial vessel embedded in agar with silica gel particles

Artificial vessels with a well defined diameter were produced by embedding metal wires in blocks of agar that was used as tissue mimicking material. Silica gel particles were added into the agar to obtain an acoustic backscattering. The artificial vessels, which were obtained after removal of the wires, were perfused with a well defined volume flow using a motor driven syringe pump. A blood mimicking fluid, which consists of particles of yeast in a solution of glycerol and water, was used for the measurements.

In Fig. 14 the envelope of echo signals sequences, which have been acquired at a flow phantom with $D = 450\,\mu$m diameter, $\alpha \approx 65°$ insonation angle and $0.177\,\text{mm}^3/\text{s}$ volume flow, is shown.

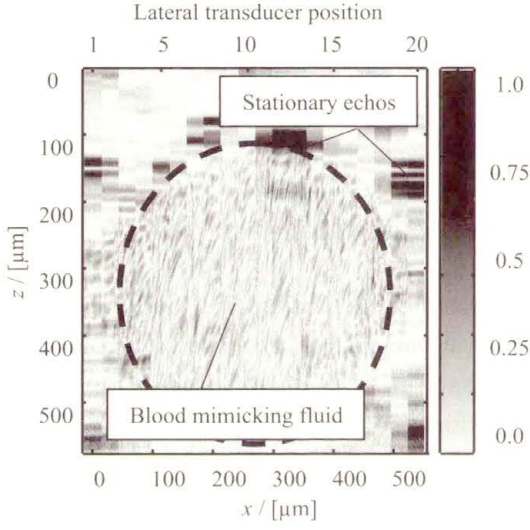

FIGURE 14. Flow phantom measurement: envelope of acquired echo signals sequences at discrete lateral transducer positions

The echo signals sequences at the discrete lateral transducer positions are shown side by side. In each sequence the echoes from $M = 50$ transmit pulses were acquired with a PRF $f_{\text{PRF}} = 800\,\text{Hz}$. Stationary echo signals from the tissue phantom are horizontal lines in the echo signal sequences. The echoes from the moving scatterers inside the blood mimicking fluid are visible as slanted lines, compare Fig. 6. A parabolic flow profile with a maximum flow velocity $v_{\text{true,max}} = 2.22\,\text{mm/s}$ is expected under the given flow conditions. The expected maximum axial and radial flow velocities are $v_{z,\text{max}} = 0.94\,\text{mm/s}$ and $v_{R,\text{max}} = 2.0\,\text{mm/s}$, respectively, with the given insonation angle.

The estimated axial and radial flow velocity profiles are shown in Fig. 15. The axial flow velocity profile estimate shows a maximum at the artificial vessel's center and smaller flow velocities towards the vessel wall. The maximum estimated axial flow velocity $\hat{v}_{z,\max} = 0.66\,\mathrm{mm/s}$ is smaller than expected. This can be explained by the given uncertainty about the actual insonation angle α in the measurement. Equivalent to the above discussed flow simulation, the variance of the estimated radial flow velocities profile is relatively high. The mean estimated radial flow velocity $\hat{v}_{R,\max} = 2.2\,\mathrm{mm/s}$ at the artificial vessel's center is in the expected range [10]:

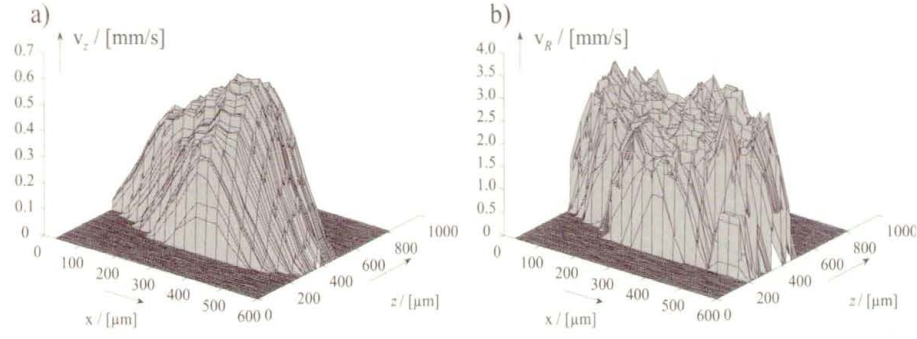

FIGURE 15. a) estimated axial flow velocity profile, b) estimated radial flow velocity profile [10]

6. In Vivo Measurements

The implemented PWD system was developed for blood flow imaging in small vessels with small flow velocities. In vivo measurements have been performed at small veins at the back of a human hand, see Fig. 1. Echo signals frames were acquired with a PRF $f_{PRF} = 1\,\mathrm{kHz}$ and an insonation angle $\alpha \approx 65°$.

In Fig. 16 a cutout of RF echo signals sequences at consecutive lateral transducer positions are shown before and after wall-filtering.

The wall-filter, which is described in Eq. (4.5), was utilized. Again, the echoes from the tissue and the vessel wall are visible as horizontal line. They are suppressed significantly after wall-filtering. The echo signal energy after the wall-filter is utilized as a measure to decide at each point in the color flow image and power mode image whether flow is visualized or not. If the energy is below a user-defined threshold, the morphological B-mode image

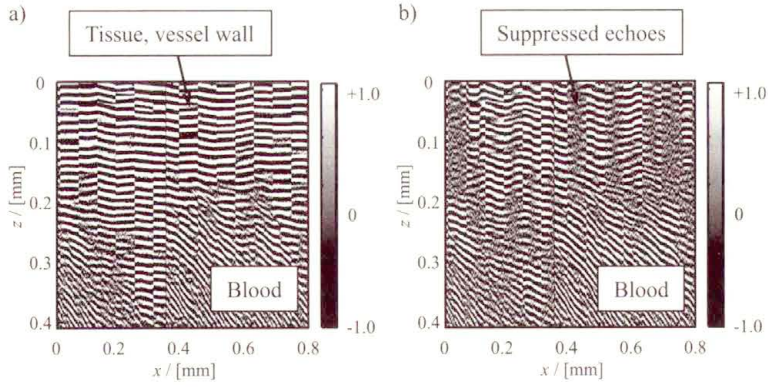

FIGURE 16. In vivo imaging: echo signals sequences: a) before wall-filtering, b) after wall-filtering

information is visualized. If the energy is larger than the threshold, the flow information is imaged.

The color flow image in Fig. 17 a) shows the mean axial flow velocity distribution over the vessel's cross section.

The maximum estimated axial flow velocity is $\hat{v}_{z,\max} \approx 5\,\mathrm{mm/s}$ In the power mode image in Fig. 17 b) the perfused cross-section is qualitatively visible. The echo signal power is the highest at the vessel's center. This is

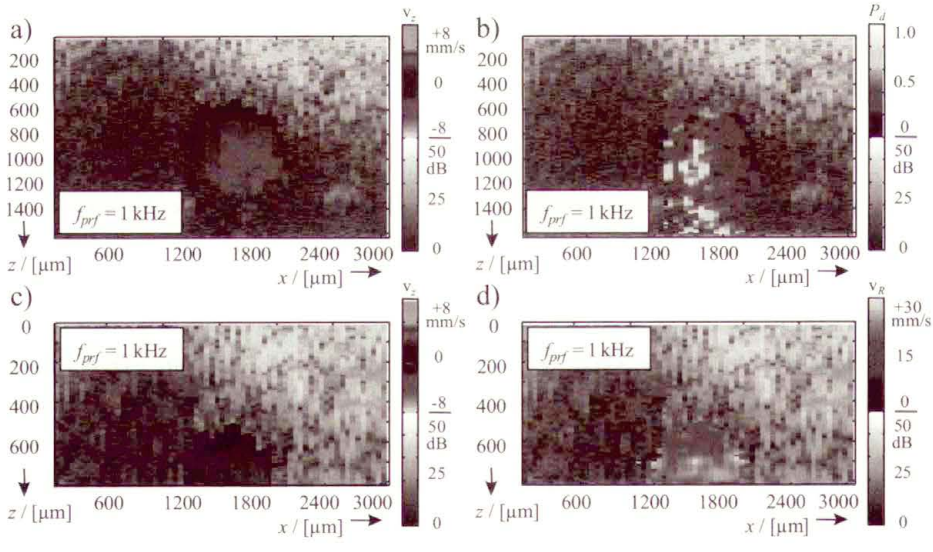

FIGURE 17. Vein at back of human hand: a) mean axial flow velocities, b) power mode, c) mean axial flow velocities, d) mean radial flow velocities.

because the signal energy after the wall filter is the higher the more backscattering blood particles are given and the higher the flow velocities are. Estimated mean axial flow velocities and mean estimated radial flow velocities are shown in Fig. 17 c) and d). Because the signal to noise ration (SNR) of acquired signals is too low at higher depths, the color flow images are shown over a more limited depth range:

The estimated mean radial flow velocities distribution shows a maximum at the vessel's center and a decrease towards the vessel wall, as well. The transducer is mechanically scanned along the lateral coordinate x in order to acquire echo signal sequences at consecutive lateral transducer positions. Because of the cyclic heart beat and the relatively long time between consecutive acquisitions, the PWD system is synchronized to the heart beat cycle. This is achieved by triggering the data acquisition at each transducer position with the output of a photo-plethysmography system, which optically measures the heart beat cycle. Under these conditions, the color flow map represents the mean flow velocities at a constant phase of the cyclic heart beat.

7. Summary and Conclusions

A concept for the utilization of high frequency and broadband ultrasound for high resolution blood flow imaging in small vessels was presented. A PWD system with a spherically focused single element transducer with 50 MHz center frequency and 80% fractional bandwidth has been designed and implemented. High frequency and broadband ultrasound is utilized in order to achieve a good spatial resolution. Transmit signals are generated with a waveform generator, and echo signals are directly sampled with a transient recorder. Transmitter and receiver are synchronized with each other to acquire data with a well defined timing reference.

Referring to the cylindrical symmetric sound beam characteristics, the true flow velocity was separated into the axial flow velocity component in the direction of sound propagation and the radial component in transverse direction. Acquired echo signals sequences were analyzed in a two dimensional space with the micro and macro time axes.

It was shown that *combined time/frequency domain* approaches for axial flow velocities estimation can advantageously be applied in the context of broadband transmit signals. Furthermore, an approach for the estimation

of the magnitude of radial flow velocities was presented. The proposed estimation techniques were evaluated by flow simulations and flow phantom measurements.

The designed PWD system was successfully implemented. Results of flow phantom measurements show that flow velocities in the range of some few mm/s in artificial vessels as small as 100 μm in diameter are reliably estimated with the proposed approaches. In vivo measurements have been performed at small veins at the back of a human hand. It was shown that axial and radial flow velocities profiles in vessels with diameters as small as about 500 μm can be assessed.

Acknowledgement

This work has been conducted at the Institute of High Frequency Engineering of the Ruhr-University Bochum, Germany. The support of Prof. Dr.-Ing. Helmut Ermert is greatly appreciated.

References

1. J.A. JENSEN, *Estimation of Blood Velocities Using Ultrasound*, Cambridge University Press, 1996.

2. D.A. CHRISTOPHER, B. G. STARKOSKI, P.N. BURNS, and F.S. FOSTER, *A high frequency pulsed-wave Doppler ultrasound system for detecting and imaging blood flow in the microcirculation*, IEEE Ultrasonics Symposium, San Antonio, Texas, 1996.

3. D.A. CHRISTOPHER, P.N. BURNS, B.G. STARKOSKI, and F.S. FOSTER, *A high frequency pulsed-wave Doppler ultrasound system for the detection of blood flow in the microcirculation*, Ultras. in Med. and Biol., **23**:997–1015, 1997.

4. D.E. GOERTZ, D.A. CHRISTOPHER, J.L. YU, R.S. KERBEL, P.N. BURNS, and F.S. FOSTER, *High frequency color flow imaging of the microcirculation*, IEEE Ultrasonics Symposium Proceedings Sendai, pp.1525–1528, 1998.

5. D.E. GOERTZ, J.L. YU, R.S. KERBEL, P.N. BURNS, and F.S. FOSTER, *High frequency 3D flow imaging of the microcirculation*, IEEE Ultrasonics Symposium Proceedings Lake Tahoe, pp.1481–1484, 1999.

6. H. ERMERT, M. VOGT, C. PASSMANN, S. EL GAMMAL, K. KASPAR, K. HOFFMANN, and P. ALTMEYER, *High frequency ultrasound (50-150 MHz) in dermatology*, [in:] Skin Cancer and UV Radiation, P. Altmeyer, K. Hoffmann, and M. Stücker, [eds.], pp.1023–1051, Springer, Berlin, Heidelberg, New York, 1997.

7. M. VOGT and H. ERMERT, *Application of high frequency broadband ultrasound for high resolution blood flow measurement*, [in:] Proceedings of the IEEE 1997 Ultrasonics Symposium, pp.1243–1246, 1997.

8. M. VOGT and H. ERMERT, *High resolution true velocity mapping with a 50 MHz pulsed wave Doppler system for dermatology*, [in:] Proceedings of the IEEE 1998 Ultrasonics Symposium, pp.1529–1532, 1998.

9. M. VOGT and H. ERMERT, *Comparison of blood flow imaging concepts with coherent and incoherent RF carriers in the 50 MHz ultrasound region for application in dermatology*, [in:] Proceedings of the IEEE 1999 Ultrasonics Symposium, pp.1499–1502, 1999.

10. M. VOGT, C. CURIO, H. ERMERT, S. EL GAMMAL, K. KASPAR, K. HOFFMANN, M. STÜCKER, and P. ALTMEYER, *Kombinierte Erfassung von axialem und transversalem Blutfluß mit einem 50 MHz-Ultraschall-B-Bild-System für die Dermatologie*, Zeitschrift für Medizinische Physik, **1**:30–36, 1999.

11. M. VOGT, H. ERMERT, S. EL GAMMAL, K. KASPAR, K. HOFFMANN, M. STÜCKER, and P. ALTMEYER, *High resolution estimation of axial and transversal bloodflow with a 50 MHz pulsed wave Doppler system for dermatology*. [in:] Acoustical Imaging, **24**, Kluwer Academic/Plenum Publishers, New York, 2000.

12. M. VOGT, A. PLUTA, and H. ERMERT, *Comparison of time and frequency domain approaches for blood velocity estimation in small vessels using high frequency ultrasound*, [in:] Proceedings of the IEEE 2000 Ultrasonics Symposium, pp.1521–1524, 2000.

13. M. VOGT, *Direct sampling and baseband conversion in Doppler systems for high-frequency ultrasound blood flow measurements*, Electronics Letters, **41**(14):789–790, 2005.

14. R.F. WAGNER, S.W. SMITH, J.M. SANDRIK, and H. LOPEZ, *Statistics of speckle in ultrasound B-scans*, IEEE Trans. Sonics and Ultras., **30**(3):156–163, 1983.

15. W. LI, A.F.W. VAN DER STEEN, C.T. LANCEE, I. CESPEDES, and N. BOM, *Blood flow imaging and volume flow quantitation with intravascular ultrasound*, Ultras. in Med. and Biol., **24**(2):203–214, 1998.

16. M. VOGT, K. KASPAR, P. ALTMEYER, K. HOFFMANN, and S. EL GAMMAL, *High frequency ultrasound for high resolution skin imaging*, Frequenz, **55**(1–2):12–20, 2001.

17. M. VOGT and H. ERMERT, *High frequency ultrasound for high resolution imaging: Technical concepts and applications in dermatology*, [in:] Proceedings of the Workshop on Ultrasound in Biomeasurements, Diagnostics and Therapy, A. Nowicki and J. Litniewski, [eds.], pp.115–121, Abiomed Lecture Notes vol.2, IPPT PAN, CoE Abiomed, Warsaw 2005.

18. M. VOGT and H. ERMERT, *Biomicroscopy of the skin utilizing high frequency ultrasound in a multi modal approach*, [in:] Proceedings of the Workshop on Ultrasound in Biomeasurements, Diagnostics and Therapy, A. Nowicki and J. Litniewski, [eds.],

pp.69–73, Inst. of Fundamental Technological Research, Polish Academy of Sciences (IPPT PAN, ABIOMED), Warsaw, Poland.

19. C. KASAI, K. NAMEKAWA, A. KOYANO, and R. OMOTO, *Real-time two-dimensional blood flow imaging using an autocorrelation technique*, IEEE Trans. Ultrason. Ferroelec. Freq. Contr., SU-**32**:458–464, 1985.

20. K.W. FERRARA, *Blood flow measurement using ultrasound*, [in.] Biomedical Engineering Handbook, J.D. Bronzion, [ed.], CRC Press, IEEE Press, pp.1099–1118, 1995.

21. K.W. FERRARA and V.R. ALGAZI, *A new wideband spread target maximum likelihood estimator for blood velocity estimation-part I: theory*, IEEE Trans. Ultrason. Ferroelec. Freq. Contr., **38**:1–16, 1991.

22. K.W. FERRARA and V.R. ALGAZI, *A new wideband spread target maximum likelihood estimator for blood velocity estimation-part II: evaluation of estimators with experimental Data*, IEEE Trans. Ultrason. Ferroelec. Freq. Contr., **38**:17–26, 1991.

23. S.K. ALAM and K.J. PARKER, *The butterfly search technique for estimation of blood velocity*, Ultrasound in Med. and Biol., **21**:657–670, 1995.